Single-shot nanosecond laser ablation of Ni in low and high viscosity liquids at different temperatures

XIAOFENG WANG, KOTA ANDO, NAN FENG, AND TAKASHI NAKAJIMA*

Institute of Advanced Energy, Kyoto University, Gokasho, Uji, Kyoto 611-0011, Japan
**Corresponding author: nakajima@iae.kyoto-u.ac.jp*

Received XX Month XXXX; revised XX Month, XXXX; accepted XX Month XXXX; posted XX Month XXXX (Doc. ID XXXXX); published XX Month XXXX

We study the ablation efficiency of nickel submerged in water, ethanol, ethylene glycol, and glycerol, and also in ambient air for reference by single-shot nanosecond laser pulses with a special interest to see whether the liquid viscosity plays an important role on the topography of ablation craters. From the characterization of surface topography with a white light interferometry-based profilometer we find a clear difference in the ablation efficiencies in ethylene glycol at room temperature and glycerol at 100 °C for which the viscosities are rather similar. This suggests that the liquid viscosity itself would not play a major role during the formation of ablation craters.

Laser ablation [1] occurs as a result of highly nonlinear interactions between a laser pulse and a target, and lots of studies have been undertaken to understand the complicated dynamics [2-21] with some recent theoretical models [22,23]. Apart from the basic interest, laser ablation is an undoubtedly versatile technique, and roughly speaking there are two ways of applications. One way is to utilize blown-out particles as a means to synthesize nanoparticles [24-37], and another way is to utilize the laser-ablated surface itself, which is usually called laser texturing or laser processing [38–40]. The former is a convenient way to synthesize nanoparticles colloids with lasers, and there are many studies on the synthesis of nanoparticles through laser ablation of solid targets in water and various organic liquids ([31,35] and references therein). As for the latter, most studies focus on the surface morphologies upon laser ablation in air, water, and organic liquids, and very few studies report the surface morphologies of laser ablation in moderate/high-viscosity liquids such as ethylene glycol [16] and glycerol [15]. We should note that not only the atmosphere (i.e., gas or liquid environments) but also the pulse duration (i.e., femtosecond, picosecond, or nanosecond duration) is an important parameter to affect the ablation dynamics with more thermal effects by nanosecond pulses.

In either case, one of the advantages to perform laser ablation in liquid lies in the enhancement of ablation efficiency. This is because ablation occurs in a very confined space surrounded by the liquid (so-called confinement effect), so that the recoil pressure upon ablation boosts the drilling of the target. Obviously laser ablation in liquids is a very complicated process, since it involves the formation of plasma and bubble consisting of both target material and liquid component in gas as well as liquid and solid phases: Under the typical laser parameters employed for laser ablation, i.e., femtosecond, picosecond, or nanosecond laser pulses with a pulse energy of sub-mJ to a few tens of mJ and spot diameter of a few tens of μm, the plasma emission lasts for tens of nanosecond to a microsecond while the bubble starts to grow about the same time, reaches the maximum size in about one or two hundred microseconds, and then collapses [31,35]. If a short (< picosecond) laser pulse with a spot diameter of nearly diffraction limit, i.e., ~1 μm is employed, the bubble lifetime can be much shorter than 100 microseconds. There are a few studies which report the influence of liquid properties on the topography of ablated surfaces, but the liquids employed in those studies are low-viscosity liquids such as water [4,6,9,15,17,20,21] and alcohol [15,18]. As for laser ablation in moderate/high-viscosity liquids to modify the surface morphology we are aware of only a few works [15,16], and in particular reference [15] was devoted to a comparative study of high energy (>300 mJ/pulse) nanosecond laser ablation of Al and Ti alloys in water, isopropanol, and glycerol at room temperature [15], and the authors concluded that the density, thermal conductivity and acoustic impedance of the liquids play a dominant role in ablation efficiency.

To investigate the influence of liquid properties on the topography of ablated surfaces single-shot rather than multi-shot laser ablation is much more effective, since, for the case of multi-shot laser ablation, possible presence of microbubbles formed by previous laser pulses and shot-to-shot change of the target surface morphology will obscure the fundamental differences caused by laser ablation in different liquids. Varying the temperature of high-viscosity liquids is also a way to highlight the role of such liquids, because their viscosities significantly decrease with increasing temperature.

In this work we carry out a comprehensive study of single-shot nanosecond laser ablation of Ni substrates in low-viscosity liquids, i.e., water, ethanol (ET), moderate-viscosity liquid, i.e.,

Table 1. Properties of the employed liquids under the atmospheric pressure. T_b: boiling point, ρ: density, η: viscosity, n: refractive index, w: beam diameter at the target, VP: vapor pressure, C: specific heat, c: speed of sound, *Z*: synthetic acoustic impedance at the interface with Ni, *P*: plasma-induced recoil pressure.

	T_b (°C)	ρ (g/cm^3)	η (mPa·s)	n	*w* (μm)	VP (Pa)	C (Jg^{-1} °C^{-1})	c (m/s)	*Z* (gcm^{-2}s^{-1})	P/P_{water}
Water (RT)	100	1.00	1.0	1.33	174	2336	4.18	1480	2.9×10^5	1.00
ET (RT)	78	0.79	1.2	1.36	176	5800	2.42	1170	1.9×10^5	0.78
EG(RT)	197	1.12	20.0	1.43	181	7	2.38	1670	3.6×10^5	1.09
EG(100 °C)		1.06	2.1	1.41	180	2005	2.74	-	-	-
GOL(RT)	290	1.26	765.0	1.48	184	0.02	2.39	1920	4.6×10^5	1.20
GOL(100 °C)		1.21	10.9	1.45	183	26	2.83	1765	4.2×10^5	1.16

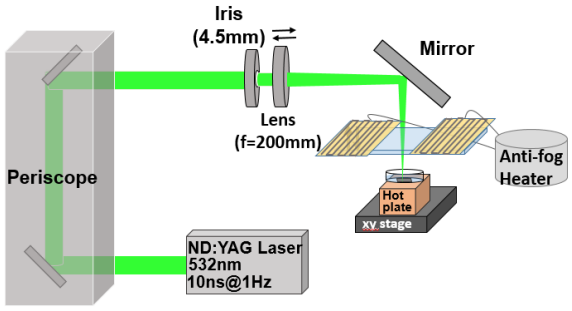

Fig. 1. Experimental setup.

ethylene glycol (EG), and high-viscosity liquid, i.e., glycerol (GOL), and also in air for reference (Table 1) with a special interest to see whether the liquid viscosity plays an important role on the topography of ablation craters, because, naively the confinement effect in a high-viscosity liquid can be stronger than that in a low-viscosity liquid. The pulse energy employed in this work is modest and similar to that employed for nanosecond laser texturing, i.e., in the range of 0.5 to 2 mJ. As for EG and GOL we perform laser ablation at RT and 100 °C. This is because the viscosities of EG at RT and GOL at RT are very different, EG at RT and GOL at 100 °C are rather similar (Table 1). Nevertheless, we find that ablation in GOL at 100 °C is more efficient than that in EG at RT, and this suggests that the liquid viscosity itself does not play a major role during the formation of ablation craters.

Figure 1 shows the experimental setup. We use Ni substrates (15 × 15 x 0.1 mm^3, Nilaco Co.) as targets of laser ablation. In order to ensure that each laser pulse interacts with an Ni surface

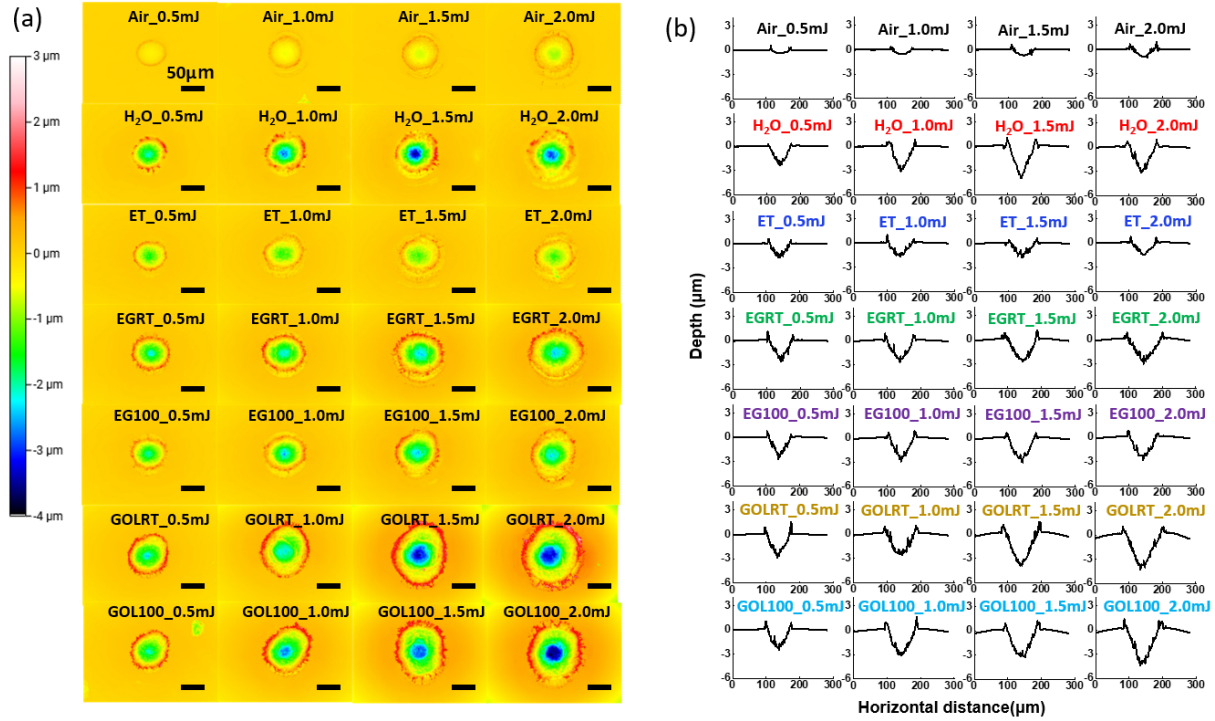

Fig. 2. (a) Morphologies of the ablation craters at different pulse energies under different environments. (b) Cross-sectional shapes of the craters cut at their centers.

with the same morphology and also to reduce the error of the crater depth measurements, Ni substrates are polished with a precision lapping machine (MA-150 Musashino Denshi, Inc.) with 1 µm diamond slurry for 30 minutes to reach the surface roughness of < 100 nm. After cleaning the polished Ni substrate with water, ethanol, and acetone, we put it in a petri dish and very quietly pour the various liquids, i.e., pure water, ethanol (ET) (>99.5%, FUJIFILM Wako), ethylene glycol (EG) (>99.5%, FUJIFILM Wako), and glycerol (GOL) (>97.0%, FUJIFILM Wako). The thickness of liquid layers above the Ni target is set to be 5 mm for all ablation experiments. For ablation we employ the second harmonic of Nd:YAG laser (INDI 30, Spectra Physics, pulse duration 8 ns, maximum repetition rate 10 Hz, maximum pulse energy 80 mJ at 532 nm, M^2~5) and operate it at 1 Hz. After the aperture set at the diameter of 4.5 mm, the laser beam is focused to the Ni target with a f=200 mm plano-convex lens, and pulse energy after the lens is controlled to 0.5, 1.0, 1.5, and 2.0 mJ with a half-wave plate and polarizing beam splitter cube. For the ablation experiments in EG and GOL at 100 °C, we employ a hot plate (Fig. 1). Heating the EG and GOL, however, results in the liquid evaporation and the mirror fogs up. To prevent the fogging, we introduce a film heater clipped on a slide glass (Fig. 1). In all liquids we adjust the focus to the best position, and repeat the single shot laser ablation of a fresh Ni surface 5 times by picking up a single laser pulse with an interval of 75 seconds using a shutter and translating the target by 1.5 mm with a motorized XY stage after each shot. All together we create only 5 x 4 = 20 ablation craters in each solution to suppress the contamination of the liquid by the ablated fragments. After completion of laser ablation in each liquid at each temperature, we clean the laser-ablated Ni substrate with pure water and dry it in air.

Shape and depth of ablation craters are measured by white light interferometry based 3D surface topography measurement system (Profilm3D, FLIMETRICS). In Fig. 2(a) we show the color-coded topographies of the ablated craters in different environments (air or liquids) at different pulse energies (0.5, 1.0, 1.5, and 2.0 mJ) and temperatures (RT or 100 °C). Initially, with the translation distance of 0.5 mm and time interval of 1 second, reproducibility of the ablation craters is not good, and this is particularly true in GOL. But after changing them to 1.5 mm and 75 second, reproducibility becomes very good even in GOL. Indeed, the choice of the relatively long translation distance of 1.5 mm and time interval of 75 seconds for the employed pulse energies is to suppress the influence of microbubbles produced by previous ablation events. We also notice that the craters formed in air are shallow at any pulse energy and similar is true for ET, while those formed in water are deeper. This implies that, although the viscosities of water and ET are very similar, topographies of the craters formed in those liquids are clearly different. To understand the observed difference between water and ET we recall that the supercritical temperature and pressure of water are 374 °C and 22.1 MPa, respectively, while those of ET are 243 °C and 6.4 MPa. Therefore, ET in the vicinity of the ablation target would be in the supercritical state for a longer time than water [41]. Since the density of supercritical fluid is between that of gas and liquid, the above consideration qualitatively explains why the topography of crater formed in ET

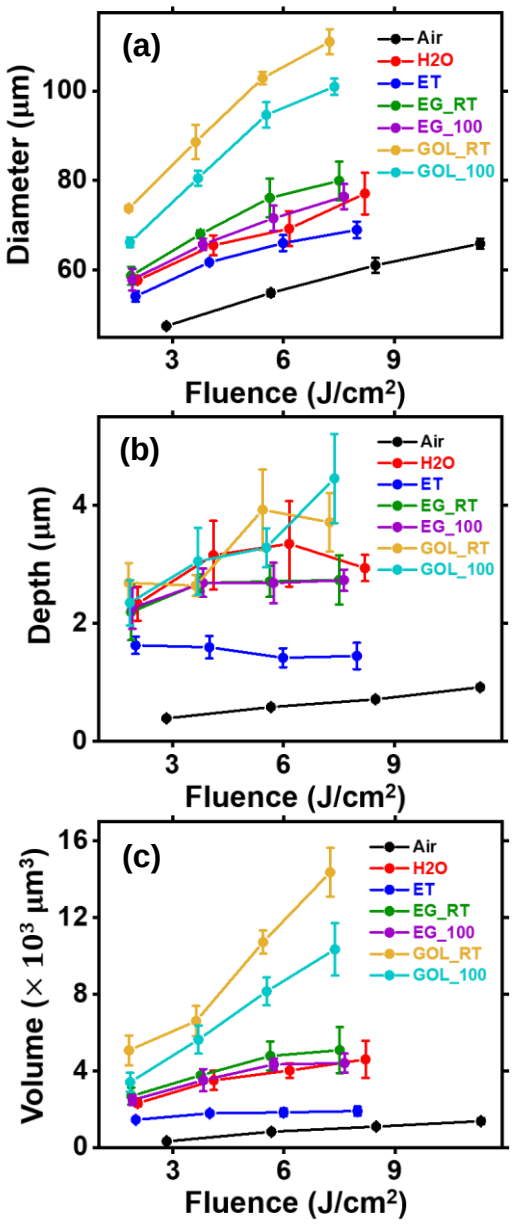

Fig. 3. Variations of (a) diameter, (b) depth, and (c) volume of ablation craters in air and different liquids as a function of laser fluence.

is between those in air and water. As for EG and GOL, while their specific heats are similar to that of ET the boiling temperatures are much higher than ET (Table 1). This explains why the confinement effects of EG and GOL are much larger than ET. It is, however, difficult to explain the topographical difference of the craters formed in EG at RT and GOL at 100 °C. While their viscosities and specific heats are both very similar (Table 1), our results in Fig. 2 show that the craters formed in EG at RT and GOL at RT are obviously different. Note that the topographies of the ablation craters presented above are much better defined than those reported in a related paper in which nanosecond 1064 nm laser pulses with 367 mJ pulse energy are employed under the tight focusing condition.

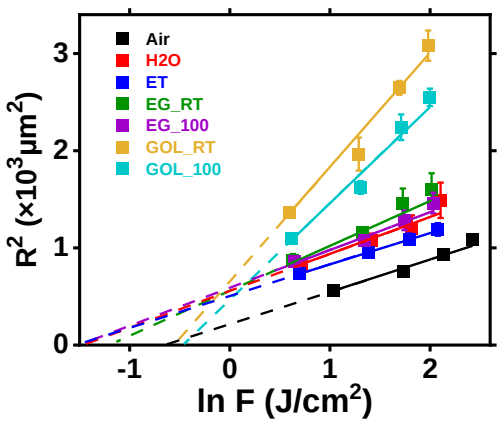

Fig. 4. Variations of the squared crater radii in air and different liquids as a function of laser fluence.

To be more quantitative, the first thing we must consider is to take into account the different laser beam diameters at the Ni target in air and different liquids. First, using the well-known formula for focusing the beam diameter at the target in air, w_{air}, is estimated to be about 150 μm. Using the relation,

$$w_{liq} = \frac{\sqrt{n}\, f'}{f} w_{air}$$

with

$$f' = n_{liq} f - (n_{liq} - 1)(f - h)$$

where w_{liq} is the laser beam diameters at the target in a liquid, while f and f' are the focal lengths of the lens entirely in air and partially in a liquid with a liquid layer thickness of h. The estimated beam diameters are listed in Table 1. We notice that the beam diameters in liquids are about 15-25 % larger in liquids than that in air, 150 μm, and they are similar in water and ET, and also in EG and GOL. We also estimate the Fresnel reflection loss at the air-liquid boundary to find that they are all 2-3.5 % and hence negligible.

Using the estimated beam diameters at the target we can estimate the laser fluences in different liquids, and plot the diameter, depth, and volume of the ablation craters that are formed under the different environments as a function of laser fluence. The results are shown in Fig. 3. As shown in Fig. 3(a), the diameter of the crater in each environment linearly increases as the laser fluence increases, and at a given laser fluence, the crater diameters are air < ET < water < EG at 100 °C < EG at RT < GOL at 100 °C < GOL at RT. Similar is true for the volume (Fig. 3(c)). In contrast, the depth of the ablation crater does not show a very clear trend (Fig. 3(b)).

Using Fig. 3(a) we plot the squared crater radius, R^2, as a function of natural logarithm of laser fluence, ln F, and the results are summarized in Fig. 4. The squared radius of the ablation crater, R^2 and laser fluence, F, are connected through [42,43],

$$R^2 = a \ln F$$

with a being a constant. Thus, the x-intercept of each line represents the ablation threshold fluence, F_{thr}, and from Fig. 4 we find that they are 0.53±0.09, 0.23±0.04, 0.21±0.01, 0.29 ± 0.08, 0.22 ± 0.06, 0.57 ± 0.03, and 0.62 ± 0.08 J/cm², respectively, in air, water, ET, EG at RT, EG at 100°C, GOL at RT, and GOL at 100 °C. Note that estimating the considering the Ablation threshold fluence of Ni in air is in reasonable agreement with the reported value [44], and those in water, ET and EG are relatively similar and lower than that in air. Interestingly, the threshold fluences in GOL at RT and 100 °C are both higher than that in air.

To find a clue to explain the different ablation efficiencies in different liquids, we now consider the pressure exerted to the target under the confined geometry through the formation of laser-induced plasma. The plasma-induced recoil pressure under the confined geometry, P, is written as [45]

$$P = 0.01\sqrt{\frac{\alpha}{2\alpha + 3}}\sqrt{Z}\sqrt{I}$$

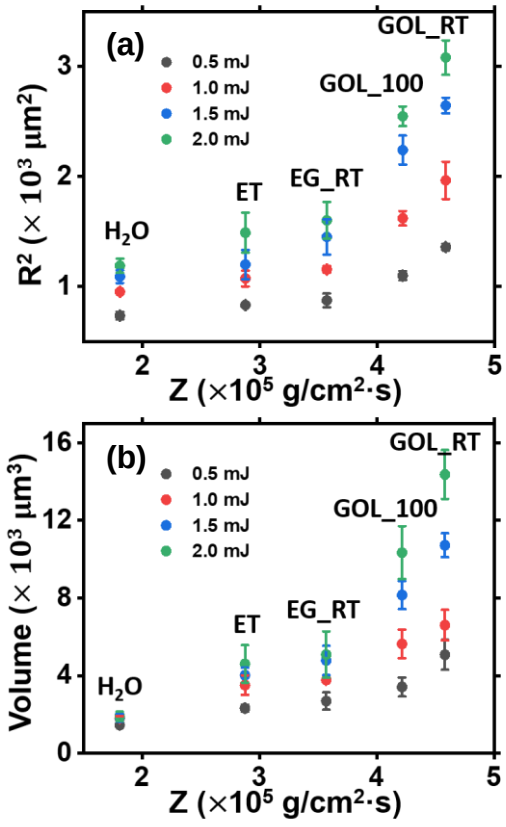

Fig. 5. Variations of the (a) squared crater radii and (b) volume of ablation craters in different liquids as a function of acoustic impedance.

with

$$\frac{2}{Z} = \frac{1}{Z_{liq}} + \frac{1}{Z_{Ni}}$$

where P is in units of GPa, and Z_{liq} and Z_{Ni} are the acoustic impedances of the liquids and Ni target with Z being a synthetic impedance of those in units of $gcm^{-2}s^{-1}$, while I is a laser intensity in units of GW/cm^2. α represents a fraction of the internal energy representing the thermal energy, and it typically takes a value of ~0.1 for 10 ns pulses [45]. The estimated synthetic acoustic impedances are listed in Table 1. Using the above expression for the plasma-induced pressure and the values of synthetic acoustic impedances listed in Table 1, we find that the relative pressures exerted to the target during the laser pulse are 1:0.78:1.09:1.20:1.16 in water, ET, EG at RT, GOL at RT, and GOL at 100 ℃, respectively. (We cannot estimate Z and hence P/P_{water} for EG at 100 ℃, since the speed of sound of EG at 100 ℃ is not available.) This order is in good agreement with the experimentally measured diameters and volumes of ablation craters presented in Fig. 3(a) and 3(c). To better see the correlation between the ablation efficiency and employed liquids we show in Fig. 5 the squared radii and volumes of the craters as a function of acoustic impedance associated with different liquids. We can clearly see the nice positive correlation. This clearly shows that the acoustic impedance or plasma-induced recoil pressure plays an important role on ablation efficiency in liquids.

In conclusion we have carried out a comprehensive study on the topographies of laser ablation craters by single-shot nanosecond laser pulses onto Ni substrates submerged in various liquids at different temperatures. We have found that the volume as well as diameter of the ablation craters well represent the ablation efficiency, and it is in increasing order of air < ET < water < EG at 100 °C < EG at RT < GOL at 100 °C < GOL at RT. We have estimated the plasma-induced recoil pressures exerted on the Ni target in the liquids to find that different ablation efficiencies in different liquids at different temperatures can be well-explained by the different recoil pressures. This suggests that, although we were initially motivated to investigate the ablation efficiencies in liquids with different viscosities, perhaps liquid viscosities themselves do not play a major role during the formation of ablation craters.

[1] D. Bäuerle, Laser Processing and Chemistry, Springer, Berlin, Heidelberg, 2011.

[2] A. Semerok, C. Chaléard, V. Detalle, J.L. Lacour, P. Mauchien, P. Meynadier, C. Nouvellon, B. Sallé, P. Palianov, M. Perdrix, G. Petite, Experimental investigations of laser ablation efficiency of pure metals with femto, pico and nanosecond pulses, Appl. Surf. Sci. 138–139 (1999) 311–314. https://doi.org/10.1016/S0169-4332(98)00411-5.

[3] X. Zeng, X.L. Mao, R. Greif, R.E. Russo, Experimental investigation of ablation efficiency and plasma expansion during femtosecond and nanosecond laser ablation of silicon, Appl. Phys. A Mater. Sci. Process. 80 (2005) 237–241. https://doi.org/10.1007/s00339-004-2963-9.

[4] J. Ren, M. Kelly, L. Hesselink, Laser ablation of silicon in water with nanosecond and femtosecond pulses, Opt. Lett. 30 (2005) 1740. https://doi.org/10.1364/ol.30.001740.

[5] S.H. Tavassoli, M. Khalaji, Laser ablation of preheated copper samples, J. Appl. Phys. 103 (2008) 1–6. https://doi.org/10.1063/1.2907955.

[6] H.W. Kang, H. Lee, A.J. Welch, Laser ablation in a liquid-confined environment using a nanosecond laser pulse, J. Appl. Phys. 103 (2008) 1–6. https://doi.org/10.1063/1.2905314.

[7] J.S. Yahng, S.C. Jeoung, Silicon substrate temperature effects on surface roughness induced by ultrafast laser processing, Opt. Lasers Eng. 49 (2011) 1040–1044. https://doi.org/10.1016/j.optlaseng.2011.04.008.

[8] L.S. Jiao, S.K. Moon, E.Y.K. Ng, H.Y. Zheng, H.S. Son, Influence of substrate heating on hole geometry and spatter area in femtosecond laser drilling of silicon, Appl. Phys. Lett. 104 (2014) 1–4. https://doi.org/10.1063/1.4875928.

[9] J.Y. Xu, H. Hu, Y.L. Lei, Morphological features of silicon substrate by using different frequency laser ablation in air and water, Appl. Surf. Sci. 317 (2014) 666–671. https://doi.org/10.1016/j.apsusc.2014.08.038.

[10] F. Bauer, A. Michalowski, T. Kiedrowski, S. Nolte, Heat accumulation in ultra-short pulsed scanning laser ablation of metals, Opt. Express. 23 (2015) 1035. https://doi.org/10.1364/oe.23.001035.

[11] H. Hu, T. Liu, H. Zhai, Comparison of femtosecond laser ablation of aluminum in water and in air by time-resolved optical diagnosis, Opt. Express. 23 (2015) 628. https://doi.org/10.1364/oe.23.000628.

[12] H. Hidai, S. Matsusaka, A. Chiba, N. Morita, Heat accumulation in microdrilled glass from ultraviolet laser ablation, Appl. Phys. A Mater. Sci. Process. 120 (2015) 357–367. https://doi.org/10.1007/s00339-015-9196-y.

[13] C. Kerse, H. Kalaycloğ Lu, P. Elahi, B. Çetin, D.K. Kesim, Ö. Akçaalan, S. Yavaş, M.D. Aşlk, B. Öktem, H. Hoogland, R. Holzwarth, F.Ö. Ilday, Ablation-cooled material removal with ultrafast bursts of pulses, Nature. 537 (2016) 84–88. https://doi.org/10.1038/nature18619.

[14] D. Qi, D. Paeng, J. Yeo, E. Kim, L. Wang, S. Chen, C.P. Grigoropoulos, Time-resolved analysis of thickness-dependent dewetting and ablation of silver films upon nanosecond laser irradiation, Appl. Phys. Lett. 108 (2016) 2–6. https://doi.org/10.1063/1.4952597.

[15] P. Ouyang, P. Li, E.G. Leksina, S. V. Michurin, L. He, Effect of liquid properties on laser ablation of aluminum and titanium alloys, Appl. Surf. Sci. 360 (2016) 880–888. https://doi.org/10.1016/j.apsusc.2015.11.080.

[16] A. Garcia-Giron, D. Sola, J.I. Peña, Liquid-assisted laser ablation of advanced ceramics and glass-ceramic materials, Appl. Surf. Sci. 363 (2016) 548–554. https://doi.org/10.1016/j.apsusc.2015.12.079.

[17] M. Akbari Jafarabadi, M.H. Mahdieh, Single and double long pulse laser ablation of aluminum induced in air and water ambient, Appl. Surf. Sci. 396 (2017) 732–739. https://doi.org/10.1016/j.apsusc.2016.11.018.

[18] S.I. Kudryashov, I.N. Saraeva, V.N. Lednev, S.M. Pershin, A.A. Rudenko, A.A. Ionin, Single-shot femtosecond laser ablation of gold surface in air and isopropyl alcohol, Appl. Phys. Lett. 112 (2018) 1–5. https://doi.org/10.1063/1.5026591.

[19] X. Sedao, M. Lenci, A. Rudenko, N. Faure, A. Pascale-Hamri, J.P. Colombier, C. Mauclair, Influence of pulse repetition rate on morphology and material removal rate of ultrafast laser ablated metallic surfaces, Opt. Lasers Eng. 116 (2019) 68–74. https://doi.org/10.1016/j.optlaseng.2018.12.009.

[20] W. Charee, V. Tangwarodomnukun, Laser ablation of silicon in water at different temperatures, Int. J. Adv. Manuf. Technol. 107 (2020) 2333–2344. https://doi.org/10.1007/s00170-020-05182-4.

[21] N.A. Smirnov, S.I. Kudryashov, A.A. Rudenko, D.A. Zayarny, A.A. Ionin, Pulsewidth and ambient medium effects during ultrashort-pulse laser ablation of silicon in air and water, Appl. Surf. Sci. 562 (2021). https://doi.org/10.1016/j.apsusc.2021.150243.

[22] B. Rethfeld, D.S. Ivanov, M.E. Garcia, S.I. Anisimov, Modelling ultrafast laser ablation, J. Phys. D. Appl. Phys. 50 (2017). https://doi.org/10.1088/1361-6463/50/19/193001.

[23] C.Y. Shih, I. Gnilitskyi, M. V. Shugaev, E. Skoulas, E. Stratakis, L. V. Zhigilei, Effect of a liquid environment on single-pulse generation of laser induced periodic surface structures and nanoparticles, Nanoscale. 12 (2020) 7674–7687. https://doi.org/10.1039/d0nr00269k.

[24] I. Lee, S.W. Han, K. Kim, Production of Au–Ag alloy nanoparticles by laser ablation of bulk alloys, Chem. Commun. 1 (2001) 1782–1783. https://doi.org/10.1039/b105437f.

[25] A. V. Kabashin, M. Meunier, Synthesis of colloidal nanoparticles during femtosecond laser ablation of gold in water, J. Appl. Phys. 94 (2003) 7941–7943. https://doi.org/10.1063/1.1626793.

[26] A. Pyatenko, K. Shimokawa, M. Yamaguchi, O. Nishimura, M. Suzuki, Synthesis of silver nanoparticles by laser ablation in pure water, Appl. Phys. A Mater. Sci. Process. 79 (2004) 803–806. https://doi.org/10.1007/s00339-004-2841-5.

[27] V. Amendola, S. Polizzi, M. Meneghetti, Laser ablation synthesis of gold nanoparticles in organic solvents, J. Phys. Chem. B. 110 (2006) 7232–7237. https://doi.org/10.1021/jp0605092.

[28] Y. Ishikawa, Y. Shimizu, T. Sasaki, N. Koshizaki, Preparation of zinc oxide nanorods using pulsed laser ablation in water media at high temperature, J. Colloid Interface Sci. 300 (2006) 612–615. https://doi.org/10.1016/j.jcis.2006.04.005.

[29] G.W. Yang, Laser ablation in liquids: Applications in the synthesis of nanocrystals, Prog. Mater. Sci. 52 (2007) 648–698. https://doi.org/10.1016/j.pmatsci.2006.10.016.

[30] V. Amendola, M. Meneghetti, Laser ablation synthesis in solution and size manipulation of noble metal nanoparticles, Phys. Chem. Chem. Phys. 11 (2009) 3805–3821. https://doi.org/10.1039/b900654k.

[31] Z. Yan, D.B. Chrisey, Pulsed laser ablation in liquid for micro-/nanostructure generation, J. Photochem. Photobiol. C Photochem. Rev. 13 (2012) 204–223. http://dx.doi.org/10.1016/j.jphotochemrev.2012.04.004.

[32] H. Zeng, X.W. Du, S.C. Singh, S.A. Kulinich, S. Yang, J. He, W. Cai, Nanomaterials via laser ablation/irradiation in liquid: A review, Adv. Funct. Mater. 22 (2012) 1333–1353. https://doi.org/10.1002/adfm.201102295.

[33] R. Streubel, S. Barcikowski, B. Gökce, Continuous multigram nanoparticle synthesis by high-power, high-repetition-rate ultrafast laser ablation in liquids, Opt. Lett. 41 (2016) 1486. https://doi.org/10.1364/ol.41.001486.

[34] C.G. Moura, R.S.F. Pereira, M. Andritschky, A.L.B. Lopes, J.P. de F. Grilo, R.M. do Nascimento, F.S. Silva, Effects of laser fluence and liquid media on preparation of small Ag nanoparticles by laser

ablation in liquid, Opt. Laser Technol. 97 (2017) 20–28. https://doi.org/10.1016/j.optlastec.2017.06.007.

[35] D. Zhang, B. Gökce, S. Barcikowski, Laser Synthesis and Processing of Colloids: Fundamentals and Applications, Chem. Rev. 117 (2017) 3990–4103. https://doi.org/10.1021/acs.chemrev.6b00468.

[36] K. Kurselis, V. Kozheshkurt, R. Kiyan, B. Chichkov, L. Sajti, Thermally assisted nanosecond laser generation of ferric nanoparticles, Appl. Phys. Lett. 112 (2018) 1–6. https://doi.org/10.1063/1.5021763.

[37] A. Letzel, M. Santoro, J. Frohleiks, A.R. Ziefuß, S. Reich, A. Plech, E. Fazio, F. Neri, S. Barcikowski, B. Gökce, How the re-irradiation of a single ablation spot affects cavitation bubble dynamics and nanoparticles properties in laser ablation in liquids, Appl. Surf. Sci. 473 (2019) 828–837. https://doi.org/10.1016/j.apsusc.2018.12.025.

[38] G. Mincuzzi, L. Gemini, M. Faucon, R. Kling, Extending ultra-short pulse laser texturing over large area, Appl. Surf. Sci. 386 (2016) 65–71. https://doi.org/10.1016/j.apsusc.2016.05.172.

[39] L.B. Boinovich, E.B. Modin, A.R. Sayfutdinova, K.A. Emelyanenko, A.L. Vasiliev, A.M. Emelyanenko, Combination of Functional Nanoengineering and Nanosecond Laser Texturing for Design of Superhydrophobic Aluminum Alloy with Exceptional Mechanical and Chemical Properties, ACS Nano. 11 (2017) 10113–10123. https://doi.org/10.1021/acsnano.7b04634.

[40] K. Sun, H. Yang, W. Xue, A. He, D. Zhu, W. Liu, K. Adeyemi, Y. Cao, Anti-biofouling superhydrophobic surface fabricated by picosecond laser texturing of stainless steel, Appl. Surf. Sci. 436 (2018) 263–267. https://doi.org/10.1016/j.apsusc.2017.12.012.

[41] N.A. Inogamov, V.A. Khokhlov, Y. V. Petrov, V. V. Zhakhovsky, Hydrodynamic and molecular-dynamics modeling of laser ablation in liquid: from surface melting till bubble formation, Opt. Quantum Electron. 52 (2020). https://doi.org/10.1007/s11082-019-2168-2.

[42] J.M. Liu, Simple technique for measurements of pulsed Gaussian-beam spot sizes, Opt. Lett. 7 (1982) 196. https://doi.org/10.1364/ol.7.000196.

[43] J. Jandeleit, G. Urbasch, H.D. Hoffmann, H.G. Treusch, E.W. Kreutz, Picosecond laser ablation of thin copper films, Appl. Phys. A Mater. Sci. Process. 63 (1996) 117–121. https://doi.org/10.1007/BF01567638.

[44] L. Torrisi, F. Caridi, D. Margarone, L. Giuffrida, Nickel plasma produced by 532-nm and 1064-nm pulsed laser ablation, Plasma Phys. Reports. 34 (2008) 547–554. https://doi.org/10.1134/S1063780X08070039.

[45] R. Fabbro, J. Fournier, P. Ballard, D. Devaux, J. Virmont, Physical study of laser-produced plasma in confined geometry, J. Appl. Phys. 68 (1990) 775–784. https://doi.org/10.1063/1.346783.